Unsteady, viscous, circular flow

Part 3. Application to the Ranque–Hilsch vortex tube

By MERWIN SIBULKIN

Convair Scientific Research Laboratory, San Diego

(Received 10 July 1961)

A new explanation of the vortex tube is presented. The proposed model leads to an equivalent unsteady-flow analysis for the development of the flow in the vortex tube. Using this analysis, radial distributions of velocity and temperature can now be calculated at successive axial positions in the tube. Many characteristics of these calculated profiles are found to be in qualitative agreement with corresponding experimental profiles. The qualitative similarity in the development of the calculated and experimental sets of profiles with axial position is considered especially significant.

A theory of vortex-tube performance based upon an idealized three-dimensional flow pattern for the vortex tube is derived. Some experiments relating the idealized vortex tube analysed to previous vortex-tube measurements are described. The performance curves obtained from the theory resemble those measured. An important additional effect predicted by the theory is that both the hot and the cold temperature differences should increase as the effective height of the inlet nozzle increases, and this result has been substantiated by experiment.

1. Introduction

The vortex tube was first mentioned in a French patent applied for by G. J. Ranque in December, 1931. A similar patent was applied for in the United States in December 1932 (Ranque 1934). The following year, Ranque (1933) read a paper to the Societe Française de Physique, and, as far as is known, this is the last reference to the vortex tube by its inventor. After this the vortex tube lay dormant until 1945 when British and American investigators rediscovered it in the laboratory of R. Hilsch at the University of Erlangen, Germany. Hilsch had begun his investigation of the vortex tube in 1944 after reading Ranque's paper; his results were published in Germany in 1946 and in the United States in Hilsch (1947). This time interest in the vortex tube remained high, so much so that by 1954 a comprehensive survey of vortex-tube publications by Westley (1954) included over a hundred references to the device; and, judging by the number of publications since 1954, interest in the vortex tube has not abated. This interest may be due to the fact that, 'Besides its possible importance as a practical device, the vortex tube presented a new and intriguing phenomenon in fluid dynamics' (Westley 1954).

A schematic drawing of the vortex tube is shown in figure 1 *a*. The inlet nozzle is tangent to the main tube which causes the entering air to acquire the vortical

motion which gives the device its name. At one side of the inlet nozzle is a fixed flow restriction called the 'cold orifice', and at the other end of the main tube there is a variable flow restriction called the 'hot valve'. These names derive from the essence of the vortex tube, namely, that the air leaving the tube through the orifice is colder than the entering air while the air leaving through the valve is hotter. The degree of heating and cooling depends upon the relative amount of air leaving each end of the tube, and is customarily plotted in terms of the parameter μ as shown in the typical performance curves of figure 1*c*. The minimum in the curve of $T_c - T_0$ vs. μ is characteristic of published measurements and will be considered later in this paper.

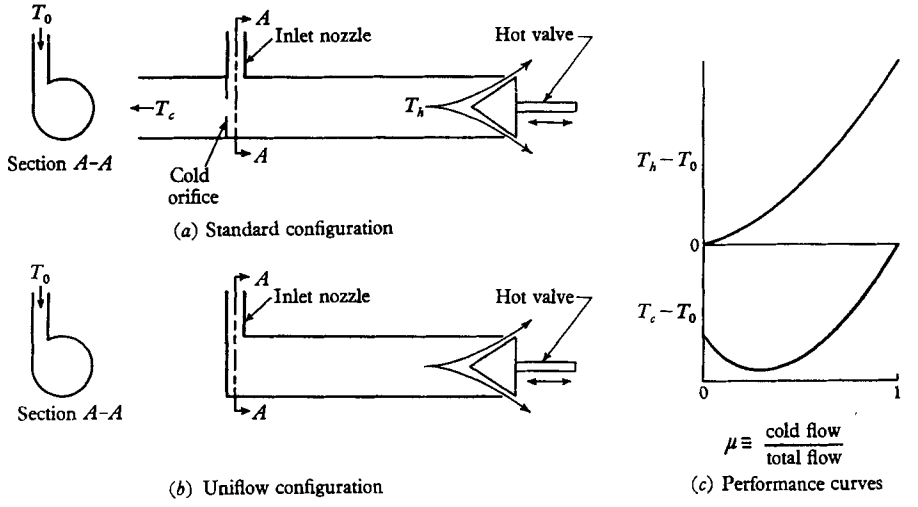

FIGURE 1. Schematic drawings and typical performance characteristics of vortex tubes.

Experimental work on the vortex tube divides itself into two main types. The first consists of parametric studies of the effects of varying the geometry of the vortex tube components on the operating characteristics of the tube, and leads to performance curves of the type shown in figure 1*c*. The earliest investigation in this category is the one by Hilsch (1947). Other major investigations of this type were published by Dornbrand (1950), Martynovskii & Alekseev (1957), Westley (1957), and Suzuki (1960).

The second type of experimental investigation concentrates on the flow within the vortex tube by measuring the pressure, velocity and temperature profiles at various stations between the inlet nozzle and the hot valve. The earliest of these was by Scheper (1951). Later investigations of this type concentrated on the operating condition $\mu = 0$ by using a 'uniflow' vortex tube (figure 1*b*) in which the tube is blocked at the cold orifice position and all the air leaves through the hot valve. Major publications in this category are Hartnett & Eckert (1957) and Lay (1959).

1.1. *Résumé of published analyses*

In his pioneering paper, Hilsch (1947) gave a qualitative description of the flow in the vortex tube and postulated an outward flow of *kinetic* energy due to internal

friction. He also suggested that the, '[hot] valve should be sufficiently far away from the nozzle. . . so that the gas reaching it will have lost most of its screw-like motion because of internal friction', a recommendation frequently overlooked by later theorists.

An analytical approach following the qualitative description of Hilsch was made by Kassner & Knoernschild (1948). They assumed that the velocity profile of the entering air was a portion of a free vortex (constant angular momentum) and that as the air moved towards the hot valve the velocity profile was converted to that of a forced vortex (constant angular velocity) by the action of viscosity. They also postulated an 'adiabatic' temperature distribution due to turbulent mixing. Then by dividing their vortex into two parts at selected values of the radius and identifying the inner and outer portions with the cold and hot flows leaving the vortex tube at corresponding values of μ, the authors obtained performance curves which agreed with Hilsch's measurements.

Another analytical approach was initiated in an appendix to Dornbrand (1950). In this approach the vortex tube is replaced by a steady, two-dimensional, driven vortex having velocity and temperature profiles which are identical in all sections perpendicular to the axis of the vortex. The Dornbrand analysis considered only the momentum equation and the transfer of energy due to shear work, but included the effect of radial flow. A 'two-dimensional vortex tube' based upon this flow model was built, but is stated to have been 'unsuccessful'.

A third analytical approach was given by Scheper (1951). He postulated a flow model based upon experimentally determined flow patterns in which the vortex tube was considered to act as a counterflow heat exchanger, and he developed a semi-empirical theory which gave results which agreed with Hilsch's measurements.

Another two-dimensional vortex analysis with only circumferential flow was made by Van Deemter (1952) who used the complete energy equation to calculate the temperature distributions corresponding to several assumed velocity distributions. By dividing his vortex into two parts at selected values of the radius, the author obtained performance curves which agreed with Hilsch's measurements.

One drawback of the two-dimensional approach to the vortex tube based upon purely circumferential flow is that the only *steady* velocity distribution which satisfies the momentum equation is that of constant angular velocity, and this leads, in the case of a stationary wall, to no velocity at all. It was perhaps consideration of this problem which led Pengelly (1957) to consider again the two-dimensional vortex with radial inflow. His analysis extended to Dornbrands's solution to include the effects of dissipation but not of heat conduction.

The most complete solution of the steady vortex has been given by Deissler & Perlmutter (1960), who include both radial and axial flow and use the complete energy equation. The solution is still essentially two-dimensional, however, in that the circumferential velocity and the temperature profiles are identical in all sections perpendicular to the axis of the vortex. By dividing their vortex into two parts at selected values of the radius, the authors obtained performance curves which agreed with Hilsch's measurements.

It is this author's opinion that none of these theories have produced velocity and temperature profiles which agree even *qualitatively* with those obtained experimentally. In the only paper in which such a comparison was made (Deissler & Perlmutter 1960), agreement could be obtained only by comparing theoretical curves based upon particular values of the radial flow parameter with experimental curves at an arbitrarily selected axial station in the vortex tube. For other values of the radial flow parameter, the analysis gave qualitatively different results.

On the other hand, widely divergent theories have given performance curves which agree with Hilsch's measurements. It follows, therefore, that an understanding of the mechanism which produces the vortex tube temperature separation phenomenon can only be obtained from a theory which predicts *both* the performance characteristics and the internal flow profiles of the vortex tube.

In the present paper, such an explanation of the vortex tube phenomenon will be advanced. The investigation falls into two divisions. In the first, §§ 3 to 5, velocity and temperature profiles are obtained using the methods developed in Sibulkin (1961*b*). These theoretical profiles are calculated with the use of the measured performance values corresponding to the experimental profiles with which they are compared. In the second division, §§ 6 and 7, an approximate theory is developed to predict the performance characteristics of the vortex tube. In both divisions, some new experimental work suggested by the analysis is presented.

2. Notation

In addition to conventional symbols for thermodynamic quantities and the co-ordinates shown in figure 2, major symbols used are defined below; minor symbols are defined where used.

a	value of s separating core and annulus
a_g	$\equiv (R-h)/R$
h	inlet nozzle height
p; p_t; p_0; p_a	static; total; supply; ambient pressure
R	vortex tube radius
s	$\equiv r/R$
T; T_t; T_0	static; total; supply temperature
v, w	circumferential and axial velocity
V	velocity corresponding to isentropic expansion from p_0 and T_0 to p_c
μ	ratio of cold mass-flow rate to total mass-flow rate
ν	kinematic viscosity
τ	$\equiv (\nu/R^2)\,t$
*	superscript denoting non-dimensional quantities defined in (7)
^	superscript denoting non-dimensional quantities defined in (12)
c	subscript denoting both value in core at inlet plane and value in cold stream leaving vortex tube
h	subscript denoting value in hot stream leaving vortex tube

3. The model of the flow and method of solution

This analysis is based upon the contention that an adequate explanation of the Ranque–Hilsch vortex tube must take into account the variation with axial position of the flow field within the tube. Consider the semi-infinite, uniflow vortex tube shown in figure 2. A cylindrical polar co-ordinate system having its z-axis along the centre-line of the vortex tube is used. The flow enters tangentially at $z = 0$, and spirals down the tube with a circumferential velocity v which decays with increasing z.† The flow leaves the tube at $z = \infty$ with zero circumferential velocity and uniform temperature. At intermediate values of z, the circumferential velocity must be zero at the centre of the tube and at the wall giving the type of velocity profile $v(r)$ sketched in figure 2. The analysis assumes that the flow is symmetrical about the z-axis, and that the vortex-tube walls are perfectly insulated.

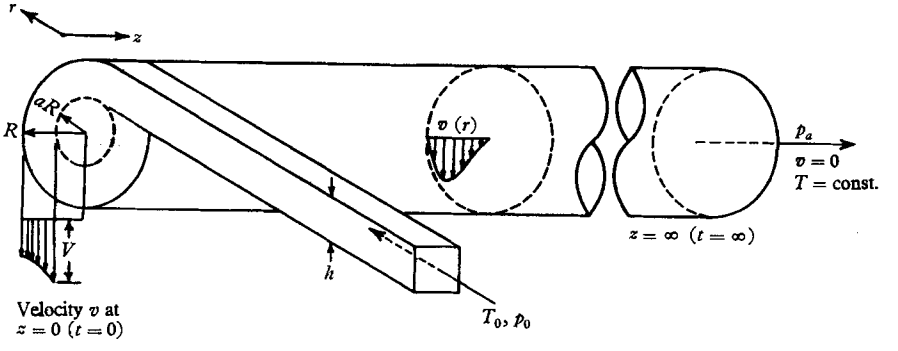

FIGURE 2. Vortex tube model used in analysis showing idealized circumferential velocity distributions.

This description of the vortex tube gives rise to a steady-flow problem in three-dimensional space which is mathematically intractable. An approximation to this flow problem, which is the key to our analysis, will now be made; viz. that this *steady*, three-dimensional flow problem may be replaced by an *unsteady*, two-dimensional problem by neglecting the shear forces associated with the axial and radial components of the velocity in comparison to the shear associated with the circumferential velocity distribution. *In this approximation we calculate the* subsequent behaviour of a fluid element which enters the vortex tube at $t = 0$, and associate increasing values of time in our analysis with increasing values of z in the vortex tube. No explicit relation between t and z will be sought. It will be found that such a relationship is not necessary to obtain the *qualitative* agreement between theory and experiment which is the object of this analysis.

3.1. *Fundamental equations and boundary conditions*

The approximation to the flow in the vortex tube described above is mathematically equivalent to the problem of unsteady, viscous, circular flow in an infinite cylinder of finite radius considered in Sibulkin (1961*b*). As in that analysis,

† The velocity profile assumed at $z = 0$ will be discussed in § 3.2.

we will assume that the fluid is a perfect gas having the equation of state $p = \rho \mathscr{R} T$ and constant values of specific heats c_p and c_v, and that the Mach number in the flow field is everywhere much less than one. Under these conditions the Navier–Stokes and energy equations can be reduced to the form (Sibulkin 1961*a*)

$$\rho r \omega^2 = \partial p / \partial r, \tag{1}$$

$$\frac{\partial \omega}{\partial t} = \frac{\nu}{r^3} \frac{\partial}{\partial r} \left(r^3 \frac{\partial \omega}{\partial r} \right), \tag{2}$$

$$c_p \frac{\partial T_t}{\partial t} = c_p \frac{\partial T}{\partial t} + \frac{\partial}{\partial t} \left(\frac{v^2}{2} \right) = \frac{1}{\rho} \frac{\partial p}{\partial t} + \frac{\nu}{r} \frac{\partial}{\partial r} \left[r^3 \frac{\partial}{\partial r} \left(\frac{\omega^2}{2} \right) \right] + \frac{k}{\rho r} \frac{\partial}{\partial r} \left(r \frac{\partial T}{\partial r} \right), \tag{3}$$

where $\omega (\equiv v/r)$ is the angular velocity and $c_p T_t (\equiv c_p T + v^2/2)$ is the total enthalpy. The terms on the right-hand side of (3) represent respectively (i) the increase in enthalpy due to compression of a fluid element, (ii) the viscous work on an element, and (iii) the net heat conduction into an element.

The boundary conditions for these equations are

$$\left.\begin{aligned} (\partial \omega / \partial r)(0, t) = 0, \quad (\partial T_t / \partial r)(0, t) = 0; \\ \text{and, for } t > 0, \qquad \omega(R, t) = 0, \quad (\partial T_t / \partial r)(R, t) = 0; \end{aligned}\right\} \tag{4}$$

where the conditions at $r = 0$ follow from the assumed symmetry of the flow field, and the condition on $\partial T_t / \partial r$ at $r = R$ follows from the assumption of perfectly insulated vortex tube walls.

3.2. *Initial conditions for the vortex tube profiles*

In order to complete the mathematical formulation of the analysis, the initial conditions must be specified. It is assumed that the flow entering the vortex tube is initially contained in an annulus having a thickess h equal to the height of the inlet nozzle (cf. figure 2), and that the fluid in the core interior to this annulus is at rest. The geometrical parameter $a_g \equiv (R - h)/R$ is related to the relative-radius r/R of the interface between the core and the annulus, and will prove of great importance in our investigation.

An idealized velocity distribution in the annulus can be obtained by assuming that the flow has expanded isentropically from a supply pressure p_0 to a core pressure p_c. Designating the velocity at the interface† $r/R = a$ as $V(p_0, p_c, T_0)$, and integrating the radial momentum equation (1) gives for $v^* \equiv v/V$

$$\left.\begin{aligned} v^* &= 0 \qquad \text{for} \quad 0 \leqslant r/R < a, \\ v^* &= \frac{a}{r/R} \quad \text{for} \quad a < r/R < 1, \end{aligned}\right\} \tag{5}$$

as shown on figure 2.

The corresponding initial conditions for the total temperature T_t are taken to be

$$\left.\begin{aligned} T_t = T &= T_c \quad \text{for} \quad 0 \leqslant r/R < a, \\ T_t &= T_0 \qquad \text{for} \quad a < r/R < 1, \end{aligned}\right\} \tag{6}$$

† In an actual vortex tube, the effective value of the interface relative-radius a may be greater or smaller than the geometrically defined relative-radius a_g; some measurements bearing on the relationship of a_g to a are reported in §7·3.

where, in this part of the paper, the initial temperature in the core T_c is considered to be one of the independent parameters of the theory. In actuality, T_c is also the temperature of the cold stream leaving the vortex tube. Predicting its value is equivalent to predicting the performance characteristics of the vortex tube and will form the central problem of the second part of this paper.

Using the numerical procedure described in Sibulkin (1961*b*) for approximating (1) to (4), solutions of these equations for the initial conditions adopted for the vortex tube will be compared with previously published measurements in the next section.

4. Comparison of calculated profiles with experiment

The calculated profiles will be expressed in terms of the following set of non-dimensional, dependent variables

$$\left.\begin{aligned} v^* &\equiv \frac{v}{V}, & p^* &\equiv \frac{p-p_a}{\frac{1}{2}\rho V^2}, \\ T^* &\equiv \frac{T-T_0}{V^2/2c_p}, & T_t^* &\equiv \frac{T_t-T_0}{V^2/2c_p}, \end{aligned}\right\} \tag{7}$$

as functions of the non-dimensional, independent variables

$$s \equiv r/R, \quad \tau \equiv (\nu/R^2)t. \tag{8}$$

The ambient pressure p_a (cf. figure 2) is equivalent to $p(s, \infty)$ and is extrapolated *a posteriori* from the computations.

4.1 *Variation of vortex tube profiles with axial position*

As mentioned in the Introduction, experimental work on vortex tube profiles has concentrated on the $\mu = 0$ operating condition obtained using the uniflow vortex tube. The most extensive measurements of this type have been reported by Lay (1959), and these will be used in comparing the measured and predicted development of the vortex tube flow profiles with axial position.

Lay's measurements were made in a lucite tube having an inside diameter of 2 in. and a length of 42 in. The air entered the tube through a single $\frac{3}{8}$ in.-diameter inlet nozzle and left the tube through a cone-shaped valve. Profiles were measured at the six axial stations tabulated on figure 3*a*; the nozzle supply pressure p_0 was 10 psig.

The theoretical profiles have been computed for a value of $T_c^* = -0{\cdot}51$ which is based upon Lay's temperature measurements (extrapolated to $z = 0$) and upon a value of V calculated for an isentropic expansion from p_0 and T_0 to p_c (where T_0 and p_c were estimated from Lay's measurements). A value of $a = 0{\cdot}55$ obtained from figure 14 for $\mu = 0$ and $T_c^* = -0{\cdot}51$ was chosen, and apologies for the use of this forward reference are made. A ratio of specific heats $\gamma = 1{\cdot}4$ and a Prandtl number $\sigma = 0{\cdot}71$ appropriate for air at these temperatures were used. Moderate variations of any of these parameters would not have affected the qualitative character of the results.

The calculated circumferential velocity profies are compared with the measured total velocities on figure 3. The total velocity was measured with a hot-wire

anemometer; unfortunately, the circumferential component of the velocity was not obtained. In comparing the two sets of curves, it should be noted that the experimental curves are reproductions of Lay's faired curves, and that his curves covered only the range of s from 0·2 to 0·95 since, '...the readings near the centre of the tube and near the wall of the tube were very erratic'. The qualitative development of the measured and calculated profiles is similar. In both cases the magnitude of the velocity maximum decreases with increasing z (or τ), while the location of the velocity maximum slowly moves towards smaller values of s.† In connexion with vortex tube explanations based on an outward flow of kinetic energy (Hilsch 1947, Kassner & Knoernschild 1948) it may be noted that, in contrast to this prediction, no such increase of velocity with axial position was measured in the outer portion of the tube.

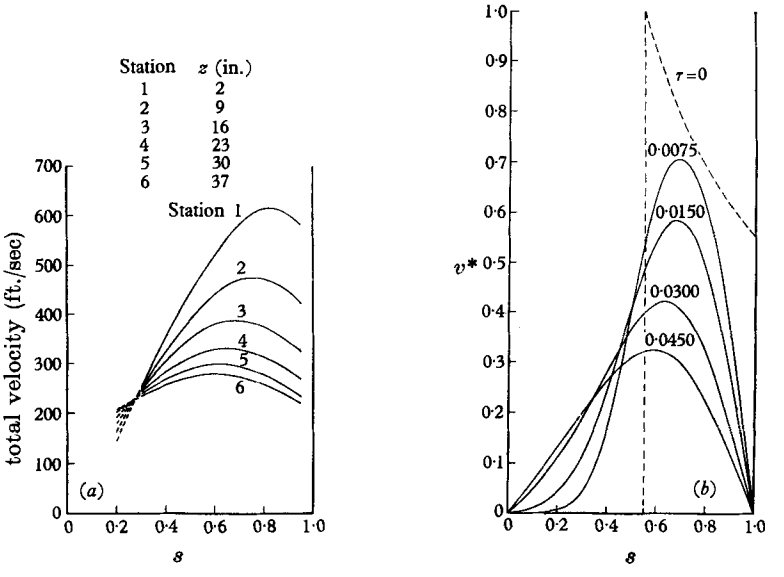

FIGURE 3. Comparison of experimental and theoretical development of velocity profiles with axial position in vortex tube. (*a*) Experiment (Lay 1959); (*b*) theory.

The measured and calculated static pressure profiles are shown on figure 4. The measurements were made with an open-ended 0·049 in. tube held perpendicular to the vortex tube axis, and the accuracy of the results obtained with such instrumentation is questionable.

The total temperature profiles are shown on figure 5. The measured temperatures are stated to be corrected thermocouple readings. The supply temperature T_0 is shown at the value suggested by Lay in a personal communication. The qualitative similarity between the two sets of profiles is evident. A feature of interest is the initial increase with z of the measured maximum total temperature and its later return towards T_0; the maxima of the calculated temperature profiles behave similarly.

† The qualitatives features of the calculated velocity profiles in the region near $s = 0{\cdot}4$ are in excellent agreement with the measured circumferential velocity profiles shown in figure 11 of Hartnett & Eckert (1957).

To complete the comparison with Lay's data, static temperature profiles are shown on figure 6. The development of these sets of profiles with axial position again shows considerable agreement. Of particular interest is the slight dip in the

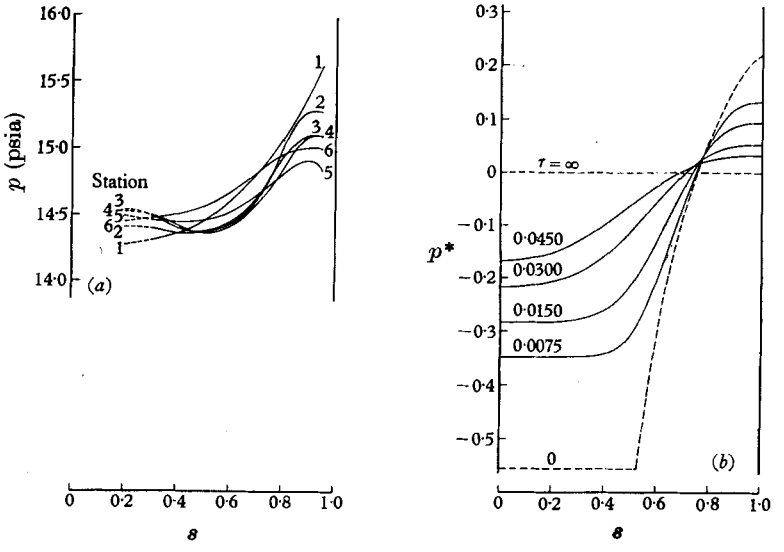

FIGURE 4. Development of static pressure profiles with axial position. (*a*) Experiment (Lay 1959); (*b*) theory.

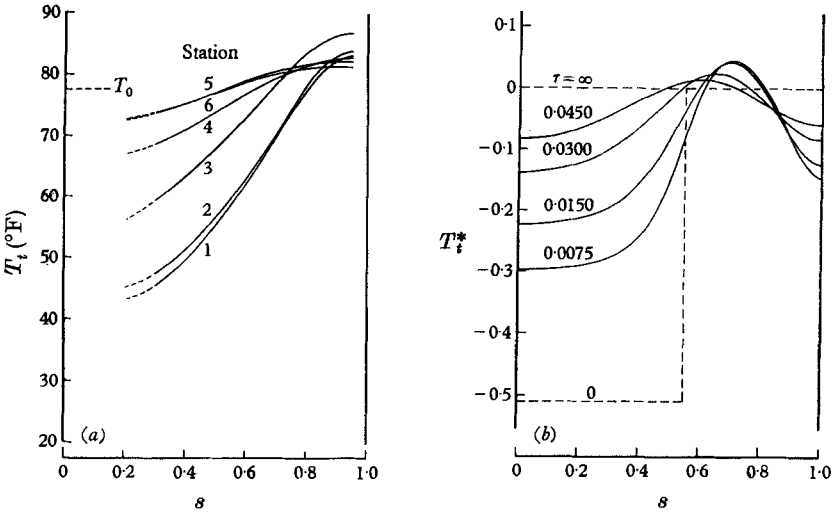

FIGURE 5. Development of total temperature profiles with axial position. (*a*) Experiment (Lay 1959); (*b*) theory.

measured profile at station 1 and the corresponding dip in the calculated profiles. More pronounced minima in the static temperature profiles will be evident in the measurements discussed in the next section.

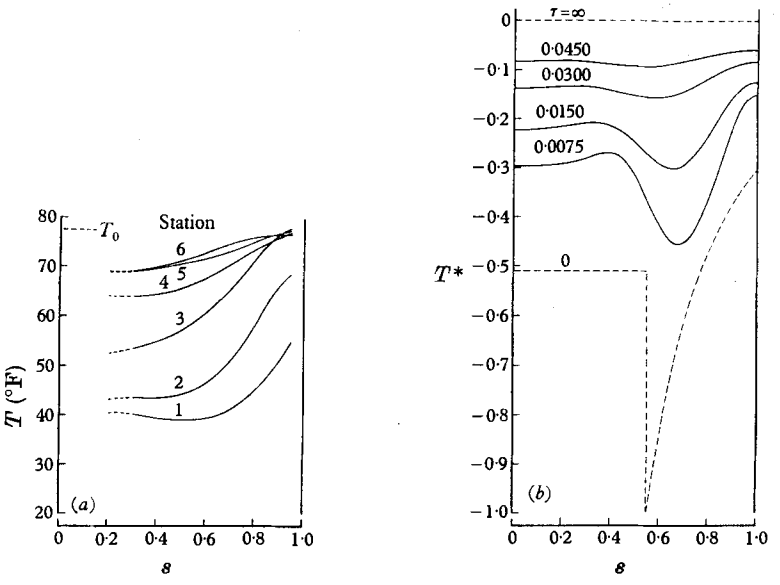

FIGURE 6. Development of static-temperature profiles with axial position. (*a*) Experiment (Lay 1959); (*b*) theory.

4.2. *Variation of vortex tube profiles with cold flow parameter* μ

The only data from which a comparison can be made of the flow profiles at a fixed position in a vortex tube for several values of μ are contained in the thesis of Scheper (1949). His measurements were made in a lucite tube having an inside

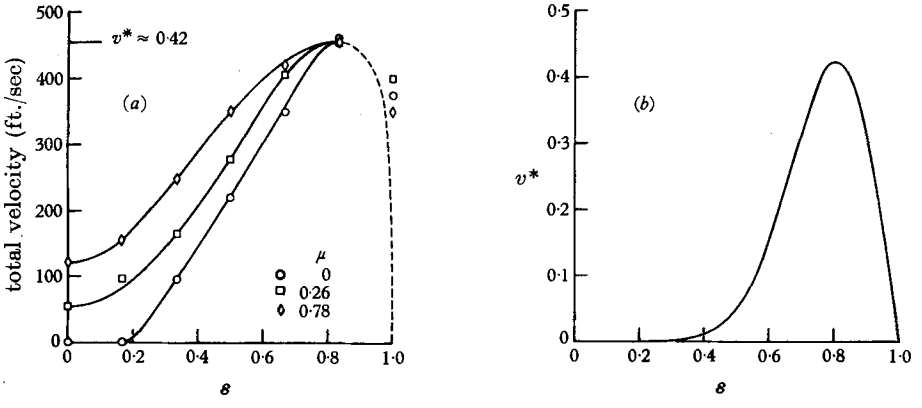

FIGURE 7. Comparison of velocity profiles at three values of cold flow parameter μ. (*a*) Experiment (Scheper 1949), $z/R = 4$; (*b*) theory, $\tau = 0{\cdot}0105$.

diameter of 1·5 in. and a length of 36 in. The flow entered the tube through a single $\frac{1}{4}$ in.-diameter inlet nozzle and left the tube through both a cone-shaped hot valve and a $\frac{1}{2}$ in.-diameter cold orifice. The profiles shown on figures 7 and 8 were measured at an axial position $z = 3$ in.; the nozzle supply pressure p_0 was 15 psig.

The corresponding theoretical profiles have been calculated for $a = 0{\cdot}75$ and for the values of T_c^* shown on figure 8; these parameters were determined by the procedure described in the previous section. In addition, a value of $\tau = 0{\cdot}0105$ was chosen by matching the maxima of the calculated and measured velocity profiles.

The measured total velocities and the calculated circumferential velocities are shown on figure 7. The velocity measurements are based upon pitot and static pressure readings. The experimental points and solid fairing lines are from

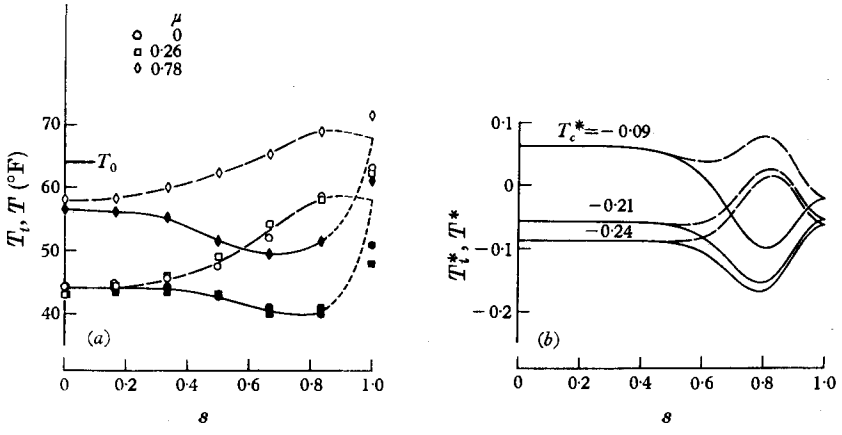

FIGURE 8. Comparison of static and total temperature profiles at three values of cold flow parameter μ. (*a*) Experiment (Scheper 1949), $z/R = 4$: – – – (open points), total temperature; —— (full points), static temperature; (*b*) theory, $\tau = 0{\cdot}0105$.

Scheper; the dashed line, which disregards the non-zero velocities at the tube wall, is the present author's. The measured velocity profiles include an axial velocity component which increases with increasing values of the cold flow parameter μ, an effect most clearly seen at $s = 0$ where the circumferential velocity should be zero at all μ. Allowing for this axial velocity effect upon the measured profiles, the theoretical prediction of a circumferential velocity profile which does not depend upon μ appears to be reasonably correct.

The experimental and theoretical temperature profiles may be compared on figure 8. The dashed portion of the curves on figure 8*a* are again based upon the assumption of zero velocity at the tube wall and upon Scheper's use of a thermocouple temperature-recovery-factor of 0·65. Within the accuracy of the data, only a single set of fairing lines were needed for the measurements at $\mu = 0$ and $\mu = 0{\cdot}26$. The static and total temperature curves for $\mu = 0{\cdot}78$ are similar to those for $\mu = 0$ and 0·26, but are at a higher temperature level; and this feature is reproduced by the calculated profiles. The minima in the static temperature profiles are clearly evident in both the measured and calculated profiles, and it was upon this negative radial temperature gradient (in the region $0{\cdot}3 < s < 0{\cdot}8$) that Scheper based his heat-exchanger theory of the vortex tube. A critique of this theory, based upon the magnitude of the static temperature differences, and some interesting remarks on vortex tube theories in general are contained in the comments of Fulton (1951) on Scheper's paper.

5. Profile measurements in the inlet nozzle plane

Previous investigators have not measured flow profiles in the region where the air enters the vortex tube (that is, at $z = 0$ in our co-ordinate system). This is unfortunate as profiles in the inlet region would be of great interest since (1) such profiles would provide a comparison with the assumed initial conditions from which our theoretical profiles develop, and (2) the steady, two-dimensional theories for the vortex tube (cf. § 1.1), which presumably apply to this inlet region†, give profiles which differ sharply from those predicted by the present theory at $z = 0$. In order to obtain such measurements a small experimental programme was undertaken.

The apparatus used is similar to that of previous investigators and is shown on figure 9. The lucite vortex tube had an inside diameter of $1\frac{3}{4}$ in. and a length of 70 in. in its uniflow configuration. This relatively long tube was run without any exit valve to approximate the semi-infinite geometry assumed in the analysis. A $\frac{1}{4}$ in.-square inlet nozzle was used for these profile measurements. Since the analysis assumes that the Mach number in the flow field is everywhere much less than one, the measurements were made at as low a supply pressure as the sensitivity of the temperature instrumentation permitted; the pressure ratio chosen was $p_0/p_c = 1{\cdot}2$.

In order to make a preliminary evaluation of the proposed division of the flow field at $z = 0$ into a core and an annulus, a flow visualization technique was developed. The result shown on figure 10, plate 1, strongly supports the quiescent core hypothesis. The photograph was made by brushing a mixture of powdered carbon and oil on the vortex tube end plate, and running the tube for about 30 sec. The instrumentation hole in the centre of the end plate was plugged during the run.

Stagnation pressure p_t and temperature T_t traverses were made through the 0·080 in. hole shown on section A–A of figure 9*a*. The probes used are shown in figure 9*b*. In operation, both the pressure and temperature probes were rotated until their readings were at a maximum. The measured stagnation pressure profile is shown on figure 11*a*. For $s > 0{\cdot}7$, the velocity was circumferential within the accuracy of the measurements.

Since no reasonably simple method of obtaining accurate static pressure measurements in this type of flow was found, the static pressure was estimated analytically. Combining the incompressible Bernoulli equation with the radial momentum equation (1) allows the static pressure to be found by integrating numerically in the relation

$$p(r) = p(0) + 2\int_0^r \frac{(p_t - p)}{r'}\,dr'. \tag{9}$$

The calculated profile was extrapolated to the tube wall using the measured value of the wall static pressure.

The velocity ratio v^* given by

$$v^* \equiv \frac{v}{V} = \left(\frac{p_t - p}{p_0 - p_c}\right)^{\frac{1}{2}} \tag{10}$$

† For example, Deissler & Perlmutter (1960, p. 189) state: 'The energy separation is assumed to take place entirely within the vortex where the tangential nozzles are located.'

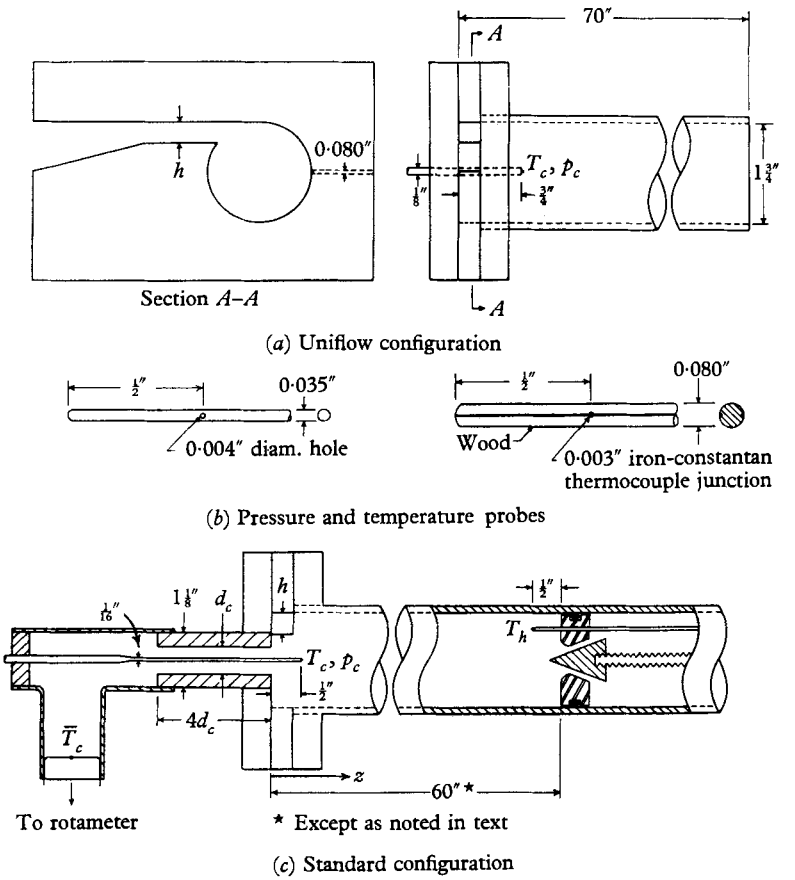

FIGURE 9. Experimental apparatus used in present vortex tube measurements.

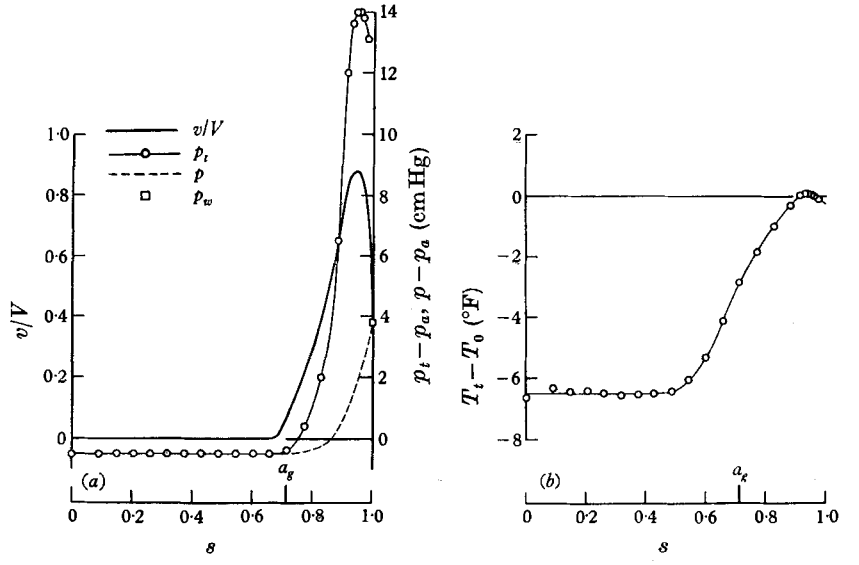

FIGURE 11. Flow distributions in the plane of the inlet nozzle. $\frac{1}{4}$ in. square nozzle, $z = \frac{1}{8}$ in., $\mu = 0$, $p_0/p_c = 1{\cdot}2$, $V = 580$ ft./sec.

is plotted on figure 11*a*. The extent of the zero velocity region is in rough agreement with the size of the core shown on figure 10, plate 1, at the circumferential location of the measurements and with the value of a_g for this inlet nozzle.

The stagnation temperature profile is shown on figure 11*b* where the measured values have been corrected for an experimentally determined probe temperature-recovery-factor of 0·95. The measurements show that the inner portion of the fluid is at a constant temperature as assumed in the analysis, but that the extent of this region is somewhat smaller than the zero velocity region. The basis for proposing such a constant temperature core is given in §6.1.

Although the temperature and velocity distributions measured outside the core at $z = 0$ do not agree with the theoretical profiles assumed at $\tau = 0$, they do resemble the profiles which would be calculated at small values of τ (for example, at values of τ small compared to 0·0075 for the case shown in figures 3*b* and 5*b*). Since the theoretical profiles at $\tau = 0$ are based upon an assumption of inviscid flow in the inlet nozzle, it is not surprising that, in an actual vortex tube, the profiles measured 'half a turn' past the inlet nozzle correspond to $\tau > 0$.

6. Theory of vortex tube performance

The results of the performance analysis advanced in this part of the paper should be viewed as even more approximate than the theoretical results of §§3 to 5 since additional, and more arbitrary, assumptions must be made to model the flow and complete the analysis.

6.1. *Basis of the theory*

The theoretical static pressure distributions in a vortex tube operating at $\mu = 0$ have been shown in figure 4*b* where increasing values of τ correspond to increasing values of z. Along the centre-line of the vortex tube ($s = 0$) these distributions show an increase of pressure with increasing distance from the inlet nozzle. This observation is the basis of the axial flow pattern proposed in figure 12*a*. According to this model, the gas on the vortex tube axis flows *towards* the inlet nozzle and diverges at $z = 0$ to form the 'core' postulated in §3·2. The assumption that all the fluid in the core at $z = 0$ is at the same temperature T_c (made in equation (6)) follows directly from this model.

The pressure in the core p_c for the uniflow configuration of figure 12*a* is a function of the supply pressure p_0 and the ambient pressure p_a. If a geometrically similar standard vortex tube operating at the same pressure ratio p_0/p_c is to be run at $\mu = 0$, then the pressure difference across the standard tube, $p_h - p_c$, must be made to equal $p_a - p_c$ by restricting the flow at the 'hot' end of the standard tube (for example, by the use of the 'hot valve' shown in figure 1*a*). In order to obtain values of $\mu > 0$, one makes $p_h - p_c > p_a - p_c$, for example, by partially closing the hot valve; the resulting axial flow pattern is shown in figure 12*b*. When the hot valve is fully closed, the tube operates at $\mu = 1$ and the pressure difference $p_h - p_c$ is greatest.

The flow patterns proposed on figure 12 are similar to those given by Scheper (1951) based on flow-visualization measurements using short threads attached to a wire stretched parallel to the axis of his vortex tube. The existence of a reverse

flow region at $\mu = 0$ has also been confirmed by the axial velocity measurements of subsequent investigators. In connexion with these flow patterns, it may be noted that the radial flow in the vicinity of the inlet nozzle is in the *outward* direction, which is opposite to that assumed in the forced vortex theories outlined in § 1.1.

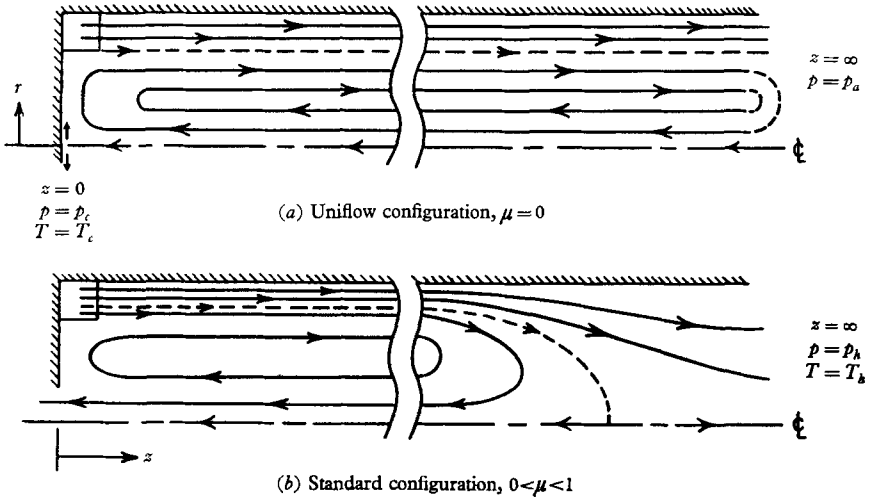

(*a*) Uniflow configuration, $\mu = 0$

(*b*) Standard configuration, $0 < \mu < 1$

FIGURE 12. Axial flow patterns used as basis for the performance analysis.

According to the model of figure 12*b*, the cold gas leaving the vortex tube at $z = 0$ came from the region of *uniform temperature* at $z = \infty$. In this respect our model differs from previous vortex tube theories, most of which obtain their temperature separation by dividing a calculated total temperature profile into a cold inner portion and a hot outer portion. In § 6.2, the performance of the vortex tube will be analyzed by calculating the decrease in temperature of a fluid element travelling along the axis of the tube from its hot to its cold end.

6.2. *Analysis of flow along the tube axis*

The change in energy of a fluid element, as shown in (3), is due to compression, viscous work, and heat conduction. At $s = 0$, the viscous work term of (3) vanishes, and the energy equation for a fluid element travelling along the vortex tube axis can be integrated from $z = \infty$ to $z = 0$ to give

$$c_p T(0) - c_p T(\infty) = [p(0) - p(\infty)]/\rho + \int_{\infty}^{0} (q/w)\, dz, \tag{11}$$

where q is the heat conducted per unit time to the element. In deriving (11), the shear work associated with the axial and radial components of velocity and changes in the kinetic energy of axial motion have been neglected in comparison to the terms retained. Defining the non-dimensional quantities

$$\hat{T} \equiv \frac{T - T_c}{V^2/2c_p}, \quad \hat{p} \equiv \frac{p - p_c}{\frac{1}{2}\rho V^2}, \quad \hat{Q} \equiv \frac{2}{V^2}\int_{\infty}^{0} \frac{q}{w}\, dz, \tag{12}$$

permits (11) to be written in the useful form

$$-\hat{T}_h = -\hat{p}_h + \hat{Q}. \tag{13}$$

In deriving explicit expressions for $\hat{p}_h$ and $\hat{Q}$, the following notation will be used. Functions of the performance parameter μ (and of the vortex tube geometry parameter a) will be written in the form $\hat{p}_h[\mu; a]$; functions based on the results of the unsteady flow analysis of § 3.1 will be written in the form $\hat{p}(s, \tau; a)$.

At $\mu = 0$, $\hat{p}_h[0; a] = \hat{p}(s, \infty; a)$; at $\mu = 1$, we *arbitrarily* assume

$$\hat{p}_h[1; a] = \hat{p}(1, 0; a)$$

where $\hat{p}(1, 0; a)$ is the highest static pressure available in the vortex tube. For intermediate values of μ, we assume that $\hat{p}_h$ increases directly with the dynamic pressure of the cold stream, that is $\hat{p}_h[\mu; a] - \hat{p}_h[0; a] \sim \rho w^2 \sim \mu^2$. Combining these assumptions gives

$$\hat{p}_h[\mu; a] = \hat{p}(s, \infty; a) + \mu^2\{\hat{p}(1, 0; a) - \hat{p}(s, \infty; a)\}. \tag{14}$$

To obtain $\hat{Q}$, we assume that the heat transferred to a fluid element as it travels from $z = \infty$ to $z = 0$ along the axis of a vortex tube operating at given values of a and $T_c^*(\mu)$ is equal to the calculated heat transfer to an element at $s = 0$ given by the unsteady flow analysis for the same values of a and T_c^*. An application of the energy equation, similar to that leading to (11), then gives

$$\hat{Q}[\mu; a] = \hat{T}(s, \infty; \hat{T}_c^*, a) - \hat{p}(s, \infty; a). \tag{15}$$

Combining (13), (14) and (15), the temperature separation between T_h and T_c can be expressed as

$$\hat{T}_h[\mu; a] = (2 - \mu^2)\,\hat{p}(s, \infty; a) + \mu^2 \hat{p}(1, 0; a) - \hat{T}(s, \infty; T_c^*, a), \tag{16}$$

where all the terms on the right-hand side of the equation may be evaluated from the unsteady flow analysis in the manner outlined below.

By integrating the radial momentum equation (1) for the initial velocity distribution (5), one easily obtains for $s \geqslant a$

$$\hat{p}(s, 0; a) = 1 - (a/s)^2, \tag{17a}$$

$$\hat{p}(1, 0; a) = 1 - a^2. \tag{17b}$$

In Sibulkin (1961*b*) it was shown that the conservation of energy requirement applied to our unsteady flow system could be expressed in the form

$$\hat{I}_E(\tau) \equiv \pi \int_0^1 \hat{E}\, ds^2 = \text{const.}, \tag{18a}$$

where (in the present notation)

$$\hat{E} \equiv \frac{c_v(T - T_c) + \frac{1}{2}v^2}{\frac{1}{2}V^2} = \frac{\hat{T}_t}{\gamma} + \frac{\gamma - 1}{\gamma}(v^*)^2. \tag{18b}$$

Evaluating $\hat{I}_E$ at $\tau = \infty$ and at $\tau = 0$ using the initial temperature conditions (6), and equating the results gives

$$\hat{T}(s, \infty; T_c^*, a) = (1 - a^2)\,T_c^* + (\gamma - 1)\,a^2 \ln(1/a^2). \tag{19}$$

Again referring to Sibulkin (1961*b*), the conservation of mass requirement can be expressed as

$$\hat{I}_\rho(\tau) \equiv \pi \int_0^1 \hat{\rho}\, ds^2 = \text{const.}, \tag{20a}$$

where, by using the perfect gas law,

$$\hat{\rho} \equiv \frac{\rho - \rho_c}{V^2/2c_p T_c} = \frac{\gamma}{\gamma - 1}\hat{p} - \hat{T}. \tag{20b}$$

After evaluating $\hat{I}_\rho$ at $\tau = \infty$ and at $\tau = 0$ using (17a) and (19) and equating the results, the terms involving T cancel and the resulting expression is

$$\hat{p}(s, \infty; a) = 1 - a^2 + (\gamma - 2)\, a^2 \ln (1/a^2). \tag{21}$$

Our final performance-equation may now be obtained by substituting (17b), (19), and (21) in (16) after eliminating T_c^* from (19) by using the overall energy balance of the vortex tube expressed as

$$\mu T_c^* + (1 - \mu)\, T_h^* = 0. \tag{22}$$

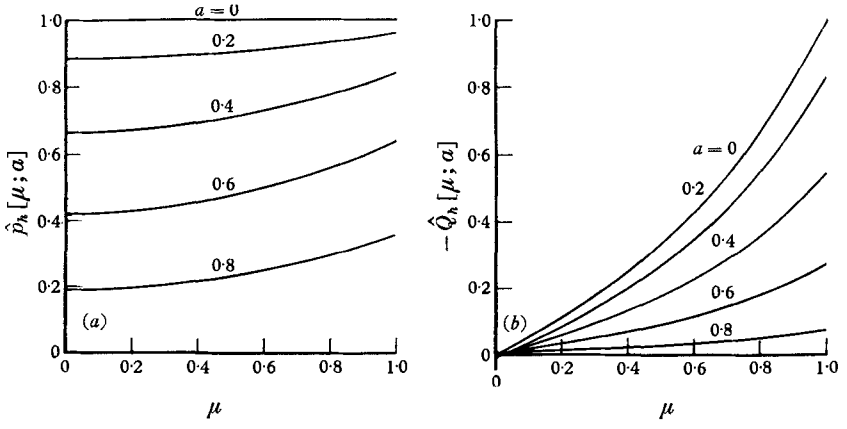

FIGURE 13. Contributions of compression and of heat conduction to the change in energy of a fluid element travelling along the vortex tube centre-line from $z = \infty$ to $z = 0$.

Applying the definitions in (7) and (12), we obtain

$$\left.\begin{aligned} T_h^* &= \mu \hat{T}_h, \quad T_c^* = -(1 - \mu)\, \hat{T}_h, \\ \hat{T}_h[\mu; a] &= \frac{2(1 - a^2) - [(2 - \mu^2)(2 - \gamma) + (\gamma - 1)]\, a^2 \ln (1/a^2)}{1 + (1 - a^2)(1 - \mu)}. \end{aligned}\right\} \tag{23}$$

The change in energy of a fluid element travelling along the vortex tube axis from $z = \infty$ to $z = 0$ has been shown to be due to compression and heat conduction, (13). The compression term $\hat{p}_h$ is given by (14), and the heat conduction term $\hat{Q}$ can be calculated from (13), (14) and (23); the results are shown on figure 13 for $\gamma = 1{\cdot}4$.

For a fixed value of a, the temperature drop due to expansion $\hat{p}_h$ which an element undergoes while travelling from $z = \infty$ to $z = 0$ increases moderately as μ increases; for a fixed value of μ, $\hat{p}_h$ increases as the radius of the core a decreases, that is, as the effective size of the inlet nozzle increases.

The temperature drop due to the net effect of heat conduction *from* the element $-\hat{Q}$ (as the element travels from $z = \infty$ to $z = 0$) is almost zero at $\mu = 0$, a result consistent with the temperature profiles shown on figure 6. As μ (and T_c^*) increases, the heat transferred from the core to the annulus increases, as would be

expected from the static temperature profiles of figure 8. And, for $\mu > 0{\cdot}05$, the magnitude of this heat transfer term $-\hat{Q}$ is larger for small values of a.

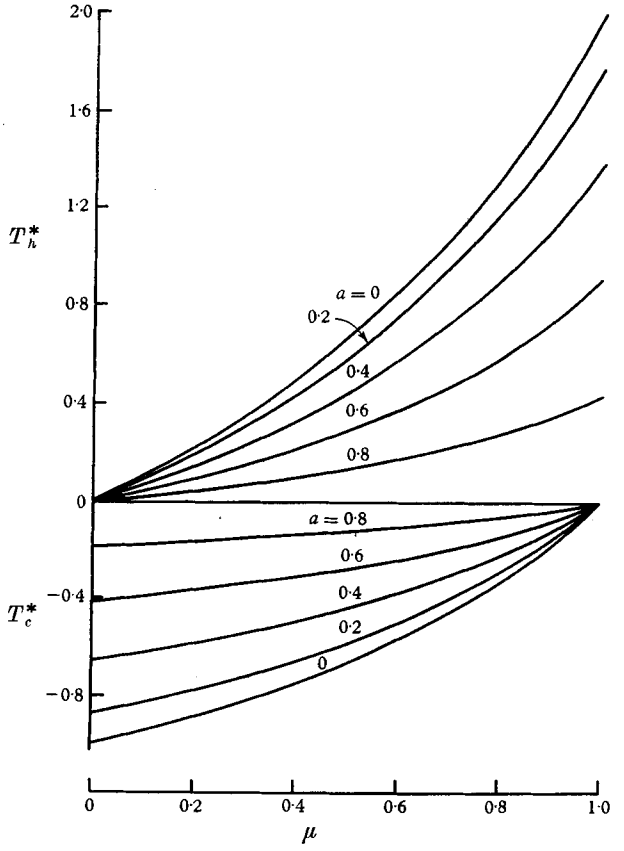

FIGURE 14. Theoretical vortex tube performance curves for several values of the effective-nozzle-height parameter a.

The combined effects of compression and heat conduction lead to the vortex tube performance curves shown on figure 14 which were obtained by evaluating (23) for $\gamma = 1{\cdot}4$. It is interesting to note that the performance analysis does not involve the Prandtl number of the gas. A new and significant prediction of this analysis is the dependence of vortex tube performance on the nozzle size parameter a. For a particular value of a the performance curves are similar to the typical experimental curves shown on figure 1*c* except for the location of the minimum value of T_c^* which occurs at $\mu = 0$ on the theoretical curves. Finally, the theory does not predict a dependence of vortex tube performance on the size of the 'cold orifice'. In order to test these predictions, the experiments reported in the next section were undertaken.

7. Performance measurements

The performance measurements discussed in this section were made with the vortex tube described in § 5. In addition to the use of the uniflow configuration shown in figure 9*a*, tests were also made with the standard vortex tube con-

figuration shown in figure 9*c*. For both configurations the inlet nozzle size was varied by using a series of nozzle plates similar to that shown as section A–A. For the standard configuration, the value of μ was varied by adjusting the conical 'hot valve', and by the use of a series of 'cold tubes' having a length to inside diameter ratio of 4:1. The vortex tube was insulated with 1 in. of Magnesia pipe insulation (not shown on the figure) to approach the insulated wall condition assumed in the analysis.

The values of T_c, p_c and T_h were measured at the locations shown on figure 9, and, as a check on the average temperature of the cold stream, $\overline{T}_c$ was read at the position shown. The temperatures were measured by iron-constantan thermocouples; the pressures probes were open-ended tubes having the diameters shown.

The measurements were made with dry, compressed air. The inlet line contained a sonic orifice which maintained the total flow-rate constant as μ was varied. The cold flow rate was measured with a rotameter, and the total flow rate was measured (with a larger rotameter) by running the tube at $\mu = 1$.

7.1. *Effect of cold flow exit size*

Although published vortex tube measurements appear to show an appreciable effect of the 'cold orifice' or 'cold tube' diameter d_c on performance, no such dependence is predicted by our theory.† The theoretical results, however, are based on the cold stream pressure p_c *upstream* of the cold flow exit, whereas the cold stream pressure p_a used by Hilsch and subsequent investigators was measured *downstream* of the cold flow exit.

When the kinetic energy of the air passing through the cold flow restriction is an appreciable fraction of the inlet air kinetic energy, p_c will be significantly greater than p_a. The effect of this difference between p_c and p_a is shown in figure 15*a* where the temperature difference $T_c - T_0$ has been plotted against both the cold tube diameter d_c and the ratio of average velocity in the cold tube $\overline{w}_c$ to average velocity in the inlet nozzle $\overline{V}_n$. (Values of $\overline{w}_c$ and $\overline{V}_n$ were obtained from the measured volume flow rates and the cold tube and nozzle areas.) Measurements were made for both $p_0/p_c = 1{\cdot}2$ and $p_0/p_a = 1{\cdot}2$. For $d_c \geqslant 0{\cdot}25$ in., the kinetic energy in the cold stream is negligible and $p_c \approx p_a$; for the smaller cold tubes, the kinetic energy ratio $(\overline{w}_c/\overline{V}_n)^2$ is appreciable and the temperature drop for $p_0/p_a = 1{\cdot}2$ is less than that for $p_0/p_c = 1{\cdot}2$. However, figure 15*b* shows that both sets of data give the same results when plotted in terms of the performance parameter $T_c^* \equiv (T_c - T_0)/(V^2/2c_p)$, where, in calculating $V(p_0, T_0, p_c)$, the measured value of p_c was used for all points. These measurements show (at least for $\mu = 0{\cdot}15$) that, for all but the largest cold tube, the value of T_c^* is reasonably independent of d_c as predicted by the theory.

For $d_c \leqslant 0{\cdot}5$ in., figure 15*a* also shows that the average cold stream temperature $\overline{T}_c$ does not differ appreciably from T_c. For the 1 in. cold tube it is interesting to note that $T_c - \overline{T}_c$ is roughly equal to the difference shown in the measured profile at $z = 0$ (figure 11*b*) between the temperatures at $r = 0$ $(s = 0)$ and $r = \frac{1}{2}d_c$ $(s = 0{\cdot}57)$.

† The analysis, however, implicitly assumes that $d_c < (R - 2h)$ so that the axial motion of all the entering air is initially in the positive z-direction.

To investigate the effect of cold tube diameter on the flow in the vortex tube, the axial velocity w† was measured along the tube centreline in the vicinity of $z = 0$ using a pitot-static tube having the same exterior dimensions as the p_c probe shown on figure 9*c*. For the smallest cold tube ($d_c = 0{\cdot}125$ in.), the calculated

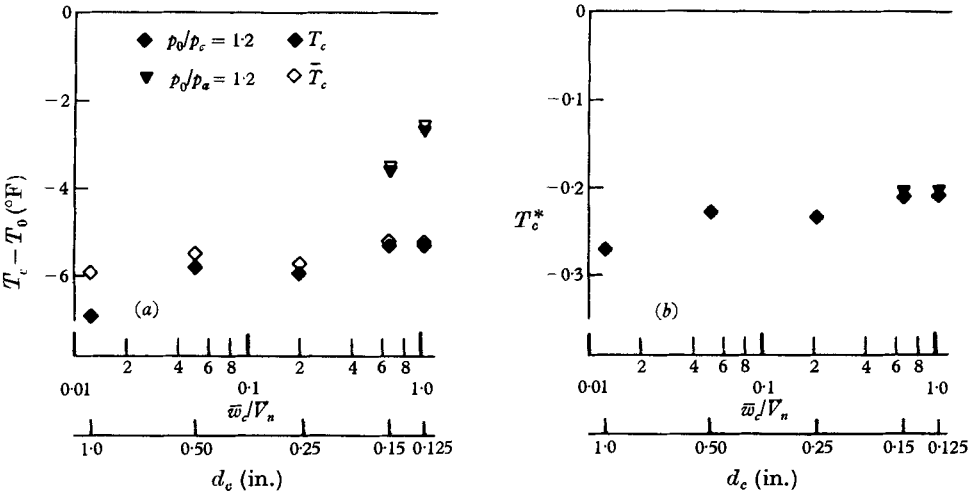

FIGURE 15. Effect of cold tube diameter d_c on cold flow temperature T_c and on T_c^*. The quantity $\bar{w}_c/\bar{V}_n$ is the ratio of the velocity in the cold tube to that in the inlet nozzle. Results for $\frac{1}{4}$ in. square nozzle, $\mu = 0{\cdot}15$.

value of $\bar{w}_c$ was 590 ft./sec and the measured value of axial velocity dropped from $w \approx 600$ ft./sec in the cold tube to a value of $w < 30$ ft./sec for $z > 0{\cdot}5$ in. For larger values of d_c, the velocity at $z = 0{\cdot}5$ was even less. From these measurements it was concluded that, for fixed values of p_0 and p_c, reducing the cold exit diameter had little effect on the flow in the vortex tube. And it was also concluded that, since $w/V \ll 1$ at $z = 0{\cdot}5$ in., differences between static and total values of temperature and pressure at that measuring point may be neglected.

For the remainder of the measurements, the 0·5 in. diameter cold tube was used.

7.2. *Location of the minimum value of T_c*

The performance curves of Hilsch (1947) showed $T_c = T_0$ at $\mu = 0$, although the author did suggest that his use of wall temperature measurements would be in error. Subsequent investigators gave performance curves of the type shown in figure 1*c* which have a minimum value of T_c at $\mu > 0$. Since these investigations (e.g. see Westley 1957) were based upon measurements of T_c downstream of the cold flow exit, their validity as the cold flow rate approaches zero (that is, as $\mu \to 0$) is questionable. On the other hand, the measurements of $T_c - T_0$ presented in figure 16 based upon measurements of T_c at $z = 0{\cdot}5$ in. show that the lowest value of T_c occurs at $\mu = 0$ in agreement with the theoretical performance curves of figure 14.

† Taken positive in the negative z-direction.

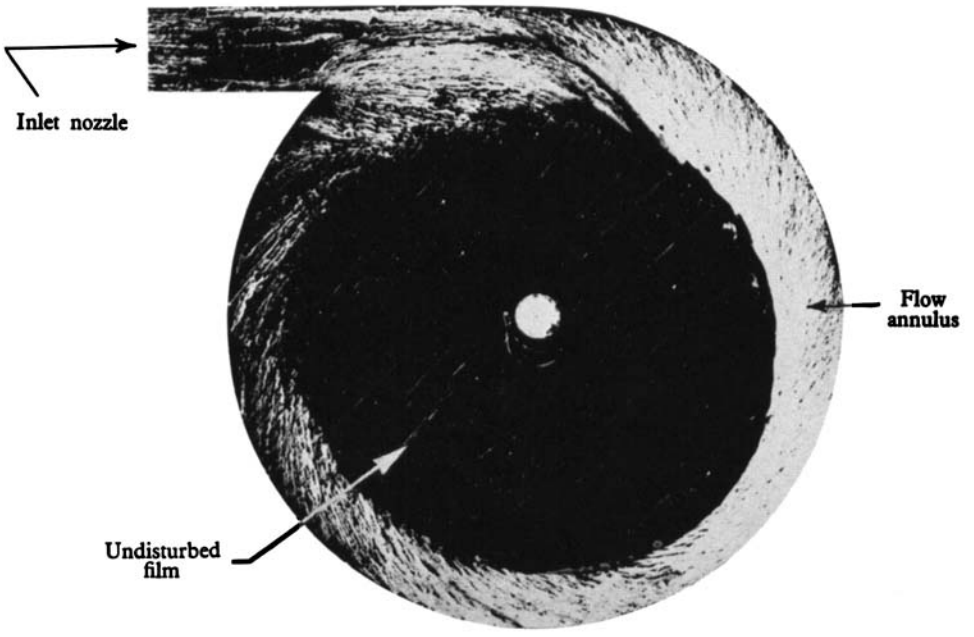

FIGURE 10. Photograph of uniflow vortex tube end-plate showing the division of the flow field in the inlet plane into a core and an annulus.

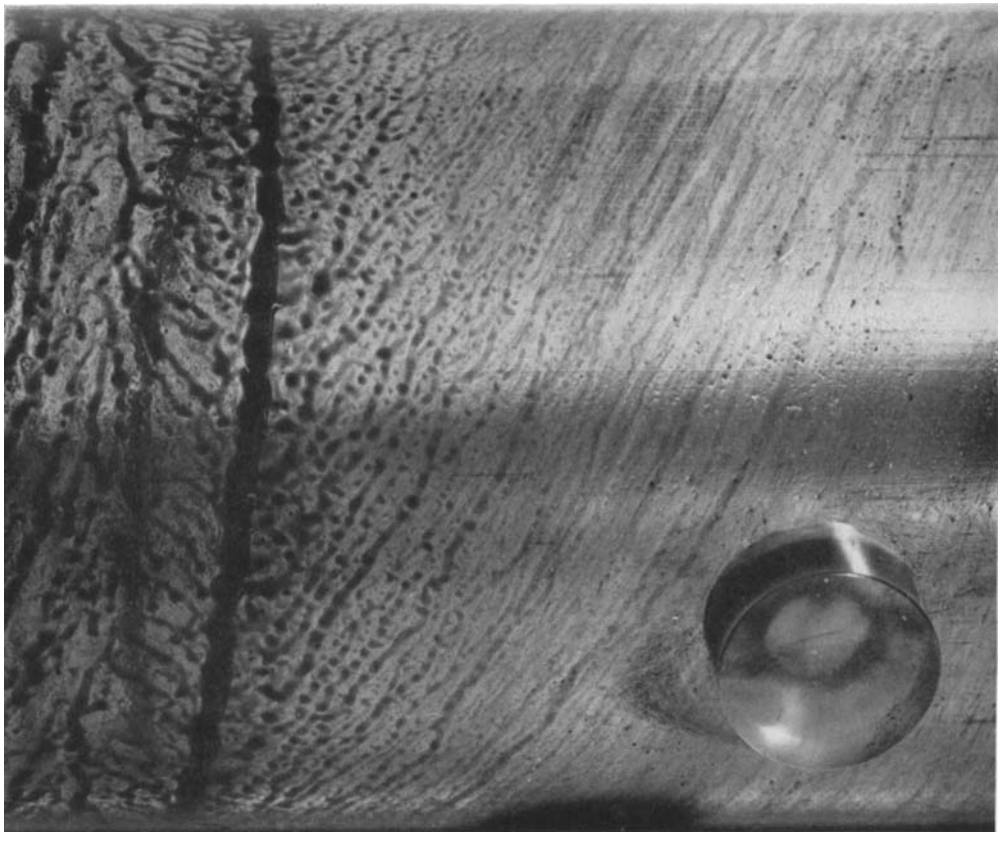

FIGURE 18. Anomalous flow pattern at $\mu = 1$ showing existence of a separation ring on the wall of the vortex tube. The hot valve is at $z = 28$ in., the ring at $z = 7$ in.; z increases toward the left.

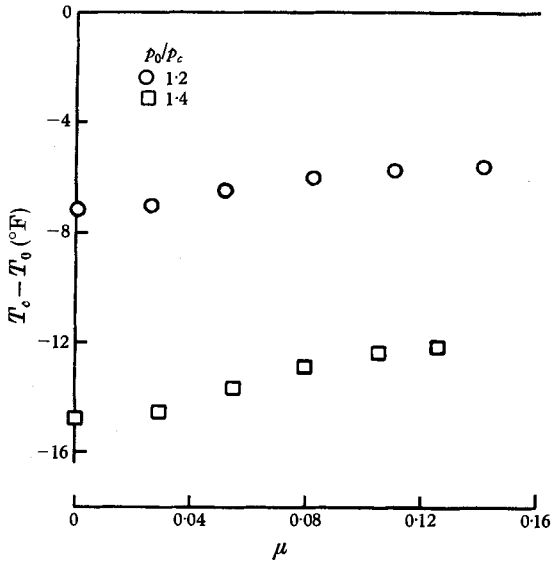

FIGURE 16. Measurements of cold flow temperature T_c in the region of small cold flow rates; $\frac{1}{4}$ in. square nozzle, $d_c = \frac{1}{2}$ in.

7.3. *Effect of inlet nozzle size*

According to our analysis, the significant geometrical parameter is the effective inlet nozzle height a. Unfortunately, no published measurements were found in which the inlet height had been systematically varied. Consequently, measurements were made at the operating conditions $\mu = 0$ and $\mu = 1$ where the effect of a on T_c and T_h respectively is greatest. The $\mu = 0$ measurements were made with the uniflow configuration shown in figure 9*a*, and T_c was measured at $z = 0{\cdot}75$ in. to reduce heat conduction along the probe and thus obtain a minimum reading. The $\mu = 1$ measurements were made with the standard configuration shown in figure 9*c*, and the hot valve was located at $z = 28$ to 30 in. for the reason given in Appendix A.

In order to investigate the relationship between the effective nozzle height parameter a and the geometric nozzle height parameter $a_g \equiv (R-h)/R$, preliminary measurements were made with several sets of rectangular inlet nozzles having width to height ratios of 2:1, 1:1 and 0·5:1. Using the flow visualization technique illustrated in figure 10 and taking a equal to the value of r/R at the edge of the core (at the circumferential position labelled 'flow annulus' in figure 10), it was found that a_g was closest to a for the square nozzles.

The experimental results for four square nozzles are shown on figure 17. The measured values of T_c^* for the $\mu = 0$ runs and of T_h^* for the $\mu = 1$ runs have been plotted against a_g; the theoretical curves of T_c^* and T_h^* versus a at $\mu = 0$ and $\mu = 1$ are taken from figure 14. The measurements show that T_h^* and $|T_c^*|$ increase as the nozzle height increases (that is, as a_g decreases) as predicted by the theory. In view of the approximate nature of the theory, however, any quantitative agreement between theory and experiment should be regarded as coincidental.

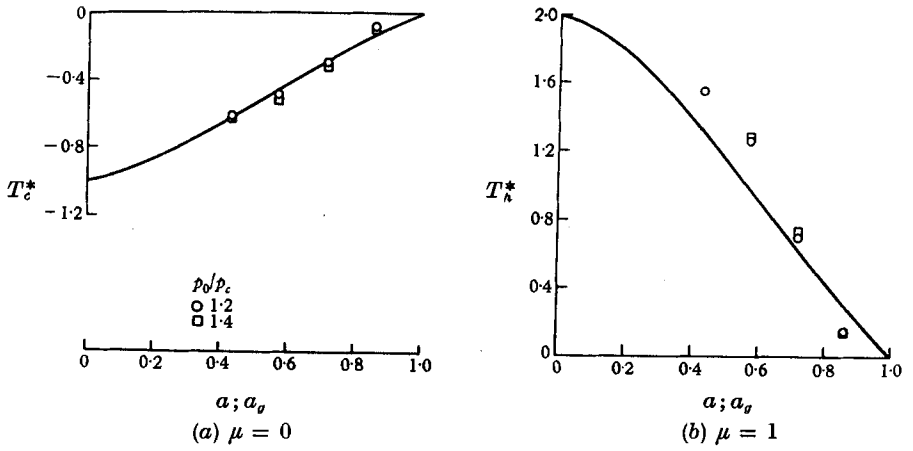

FIGURE 17. Comparison of measured and predicted effects of inlet nozzle size on the cold and the hot temperature differences produced in the vortex tube; $d_c = \frac{1}{2}$ in.

8. Summary of results

A new explanation of the Ranque–Hilsch vortex tube has been presented based upon these two concepts: (1) that the flow in the inlet plane may be divided into an annulus and an initially quiescent core, and that the subsequent velocity and temperature distributions may be calculated by an equivalent unsteady-flow analysis; and (2) that the temperature separation between the hot and cold streams leaving the vortex tube may be found by calculating the change in energy of a fluid element travelling along the centre-line of the vortex tube from its hot to its cold end (cf. figures 2 and 12).

As a result of these calculations, the following qualitative picture of the energy transfer processes in the vortex tube is obtained. When the cold flow is zero ($\mu = 0$), the amount of heat conducted from the core to the gas in the annulus is small (figure 13*b*) and as the gas in the annulus spirals along the vortex tube its decrease in energy due to expansion is balanced by an increase in energy due to viscous work (cf. equation (3)). Thus the total temperature of a fluid element in the annulus remains roughly constant (figure 5) and it leaves the vortex tube at the same total temperature at which it entered—as it must, for $\mu = 0$, to satisfy the conservation of energy requirement. Concurrently, as a consequence of the negative axial pressure gradient which exists near the centre of the vortex tube (figure 4), the gas in the centre of the tube flows towards the inlet plane (figure 12) and loses energy due to expansion. Consequently, it reaches the inlet plane with a total temperature which is less than that of the gas entering the vortex tube.

According to the analysis, the circumferential velocity distribution, and hence the viscous work term, is independent of μ. As the cold flow rate increases ($\mu > 0$), the pressure at the hot stream exit of the vortex tube increases and hence the decrease in energy of the gas in the annulus due to expansion decreases. In addition, as the cold flow rate increases, an increasing amount of heat is conducted from the core to the annulus (figure 13*b*). These two factors cause the total temperature of the gas in the annulus to increase as it travels towards the hot

stream exit, and this gas leaves the vortex tube at a total temperature exceeding the inlet total temperature. The total temperature of the gas in the centre of the vortex tube still decreases as it travels towards the cold stream exit; but the temperature of this gas at the inlet plane, while lower than the total temperature of the entering gas, is not as low as it was for $\mu = 0$.

The effects of these energy transfer processes on the operating characteristics of the vortex tube are given in the theoretical performance curves of figure 14. Although the analysis assumes molecular transport of momentum and energy, the use of turbulent transport coefficients would not affect these performance curves (cf. Appendix B), although it would affect the profiles within the vortex tube.

Some consequences of the theory have been compared with published profile measurements and with some measurements made as part of this investigation with the following results:

The division of the flow in the inlet plane into an annulus and a relatively quiescent, constant-temperature core, as assumed in the analysis, is confirmed by the experimental results shown on figures 10 and 11.

Many of the qualitative features which the measured velocity and temperature profiles in the vortex tube exhibit have been reproduced in the profiles predicted by the theory. A comparison of the development of the measured and calculated profiles with increasing distance from the inlet nozzle is shown on figures 3 to 6, and a comparison for several cold flow rates is shown on figures 7 and 8.

Measurements of vortex tube performance specifically aimed at determining the cold stream temperature as the cold flow rate approaches zero have shown that the lowest temperature occurs at $\mu = 0$ as predicted by the theory (figures 16 and 14). Another qualitative feature of the proposed theory is the absence of any explicit dependence of the calculated vortex tube performance parameters T_c^* and T_h^* on the cold flow exit diameter. When the cold flow exit diameter d_c is decreased while the pressure ratio p_0/p_a is maintained constant, the effective pressure ratio driving the vortex flow p_0/p_c decreases and hence the temperature difference $T_c - T_0$ decreases (figure 15*a*). On the other hand, the non-dimensional temperature differences T_c^*, which are based upon p_c, are relatively independent of d_c (figure 15*b*) as proposed by the theory.

The geometrical parameter which directly affects vortex tube performance, according to the theory, is the effective height of the inlet nozzle. As the inlet height increases, the radius of the core a decreases, and the analysis predicts that both the hot and cold temperature differences T_h^* and $|T_c^*|$ should increase (figure 14). Performance measurements with a series of square inlet nozzles (figure 17) gave results which substantiate this prediction.

It is a pleasure to acknowledge the assistance of Mr N. Fong in performing the experiments reported here.

Appendix A. Flow pattern at $\mu = 1$

For the tests conducted at $\mu = 0$ to 0·15, the hot valve was located at $z_h = 60$ in. to approximate the semi-infinite geometry assumed in the analysis. As $\mu \to 1$, however, this configuration gave rise to an unsteady type of flow.

Tests at $\mu = 1$ showed that, as z_h was increased, a transition to unsteady flow occurred for $z_h > 30$ in. If z_h was then reduced, an anomalous, steady-flow pattern was obtained in which the flow separated from the walls of the vortex tube at a value of $z < z_h$. Such a separation ring is shown in figure 18, plate 2, which was obtained with the powdered carbon and oil technique. The use of this technique also showed that the unsteady flow was associated with an axial oscillation of the position of the separation ring. For the performance measurements at $\mu = 1$, the hot valve was located at $z_h < 30$ in. to maintain a normal flow pattern.

Appendix B. Effects of some turbulent flow assumptions on the results of the theory

Many investigators have suggested that the flow in the vortex tube would be of a turbulent nature. Indeed, preliminary hot-wire measurements in our vortex tube at $z/R = 6$ showed that the turbulence level, relative to the maximum mean velocity at that station, varied from 3 % in the core to 7 % in the annulus.

Published turbulent vortex analyses have assumed that the eddy viscosity ϵ and the eddy conductivity κ were constants, and that the turbulent heat transfer rate q_t was given by

$$q_t = -\kappa\left(\frac{\partial t}{\partial r} - \frac{\gamma - 1}{\gamma}\frac{T}{p}\frac{\partial p}{\partial r}\right), \tag{B 1}$$

a formula first explicitly stated by Van Deemter (1952).

Application of these assumptions to our analysis would leave the velocity profiles unchanged after redefining the time co-ordinate as $\tau \equiv (\epsilon/R^2)\,t$. Because of (B 1), however, the temperature profiles in regions having appreciable pressure gradients would be altered. Since the performance analysis (§ 6.2) depends only on the assumed initial conditions and conservation of mass and energy, use of these turbulent flow assumptions would not affect our calculation of vortex tube performance.

REFERENCES

Deissler, R. G. & Perlmutter, M. 1960 Analysis of the flow and energy separation in a turbulent vortex. *Int. J. Heat & Mass Transfer*, **1**, 173–91.

Dornbrand, H. 1950 Theoretical and experimental study of vortex tubes. *Air Force Tech. Rep.*, no. 6123 (Republic Aviation Corporation).

Fulton, C. D. 1951 Comments on the vortex tube. *Refrigerating Engineering*, **59**, 984.

Hartnett, J. P. & Eckert, E. R. G. 1957 Experimental study of the velocity and temperature distribution in a high-velocity vortex-type flow. *Trans. ASME*, **79**, 751–8.

Hilsch, R. 1947 The use of the expansion of gases in a centrifugal field as cooling process. *Rev. Sci. Inst.* **18**, 108–13 (translation from *Z. Natur.*, 1946, **1**, 208–14).

Kassner, R. & Knoernschild, E. 1948 Friction laws and energy transfer in circular flow. *Wright–Patterson Air Force Base, Tech. Rep.* no. F-TR-2198-ND.

Lay, J. E. 1959 An experimental and analytical study of vortex-flow temperature separation by superposition of spiral and axial flows. *J. Heat Transfer*, **81**, 202–22.

Martynovskii, V. S. & Alekseev, V. P. 1957 Investigation of the vortex thermal separation effect for gases and vapors. *Soviet Phys.-Tech. Phys.* **1**, 2233–43, translated from *Zhur. Tekh, Fiz.*, 1956, **26**, 2303–15.

PENGELLY, C. D. 1957 Flow in a viscous vortex. *J. Appl. Phys.* **28**, 86–92.

RANQUE, G. J. 1933 Experiences sur la detente giratoire avec productions simultanées d'un echappement d'air chaud et d'un echappement d'air froid. *Bulletin Bi-Mensuel de la Societe Française de Physique*, 2 June 1933, 112, S–115, S. Also translated as *General Electric Co., Schenectady Works Library*, T.F. 3294 (1947).

RANQUE, G. J. 1934 Method and apparatus for obtaining from a fluid under pressure two currents of fluids at different temperatures. *United States Patent Office*, no. 1, 952, 281.

SCHEPER, G. W. 1949 Flow patterns and a heat transfer theory for the vortex heating and refrigerating tube. Master's thesis, Union College, Schenectady.

SCHEPER, G. W. 1951 The vortex tube—internal flow data and a heat transfer theory. *Refrigerating Engineering*, **59**, 985–9, 1018.

SIBULKIN, M. 1961*a* Unsteady, viscous, circular flow. I. The line impulse of angular momentum. *J. Fluid. Mech.* **11**, 291–308.

SIBULKIN, M. 1961*b* Unsteady, viscous, circular flow. Part 2. The cylinder of finite radius. *J. Fluid Mech.* **12**, 148–58.

SUZUKI, M. 1960 Theoretical and experimental studies on the vortex-tube. *Sci. Papers I.P.C.R. (Japan)*, **54**, 43–87.

VAN DEEMTER, J. J. 1952 On the theory of the Ranque–Hilsch cooling effect. *Appl. Sci. Res.* A, **3**, 174–96.

WESTLEY, R. 1954 A bibliography and survey of the vortex tube. *College of Aeronautics, Cranfield, Note*, no. 9.

WESTLEY, R. 1957 Vortex tube performance data sheets. *College of Aeronautics, Cranfield, Note*, no. 67.